Received: 10 December 2020 | Revised: 29 June 2021 | Accepted: 13 July 2021

DOI: 10.1002/aic.17378

SEPARATIONS: MATERIALS, DEVICES AND PROCESSES

AIChE JOURNAL

Calculation of the flux density function for protein crystals from small scale settling and filtration experiments

Benjamin Radel | Tu Hoang Nguyen | Hermann Nirschl

Institute of Mechanical Process Engineering and Mechanics, Karlsruhe Institute of Technology, Karlsruhe, Germany

Correspondence
Benjamin Radel, Institute of Mechanical Process Engineering and Mechanics, Karlsruhe Institute of Technology, Karlsruhe, Germany.
Email: benjamin.radel@kit.edu

Funding information
Deutsche Forschungsgemeinschaft (DFG), Grant/Award Numbers: NI 414/26-2, NI 414/26-1, SPP 1934

Abstract

Development and engineering of protein crystals regarding mechanical stability and crystallizability occurs on a small scale. Later in the process chain of industrial production however, filtration properties are important to separate the crystals from mother liquor. Many protein crystals are sensitive to mechanical stress which is why it is important to know the filtration behavior early on. In this study, we analyze settling and filtration behavior of isometric, rod-like and needle shaped lysozyme and rod-like alcohol dehydrogenase (ADH) crystals on a small scale using an optical analytical centrifuge. Needle shaped lysozyme and rod-like ADH crystals show compressible material behavior. With the results from settling and filtration experiments, the flux density function is calculated and modeled which can be used to describe the whole settling and permeation process in dependency of the solids volume fraction. This is also an issue for simulations of industrial processes.

KEYWORDS
filtration, flux density function, protein crystals

1 | INTRODUCTION

The improvement of bulk protein crystallization for purification or formulation is subject of current research. Crystalline proteins are advantageous compared to dissolved or amorphous solids because of their extended shelf life or modified drug release properties.[1,2] The implementation of a crystallization step in the downstream process chain for protein purification and formulation is discussed in literature by Hubbuch et al.[3] and Hekmat et al.[4] In recent research either the proteins were modified to improve or enable crystallization, or the crystals itself were altered to enhance mechanical stability.[5–7] Nowotny et al.[5] and Hermann et al.[6] identified crucial amino acids for crystallization in the sequence of the protein alcohol dehydrogenase from *Lactobacillus brevis in* a rational crystal engineering approach using a molecular dynamics model. They confirmed their findings with experimental results for three different mutants with improved crystallizability. Grob et al.[8] demonstrated the applicability of technical crystallization in downstream processing with the protein alcohol dehydrogenase. Kubiak et al.[7] used cross-linking of crystals, which drastically enhanced the crystal's ability to withstand mechanical stress. Kubiak et al.[9] reported anisotropic mechanical properties for cross-linked halohydrin dehalogenase crystals and investigated the effect of cross-linking time on crystals hardness and Young's modulus. Crystal breakage at pressures below 1×10^5 Pa for native lysozyme crystals, which negatively affects the filtration behavior of such particle systems has been previously reported by Cornehl et al.[10,11]

Filtration is a common procedure to separate solids from a liquid for further processing.[12] Hence, filtration is also suitable to separate protein crystals from saturated mother liquor. Cake forming filtration processes are well characterized and several models describing filtration parameters and cake properties may be found in literature.[13–19] Existing traditional filtration setups are changing to meet the challenges in pharmaceutical applications (integrated compact filtration devices[20,21]) or to reduce the amount of sample required in early product development. Performing standard laboratory experiments to

characterize filtration properties, for example, according to VDI 2762,[22] usually requires liters of suspension or fluid. Those amounts are not available in early product development like protein or crystal modification. This research is conducted on a much smaller scale ranging from micro- to milliliters. Investigating filtration properties of protein crystals on an early stage of process development therefore requires a much smaller laboratory setup. Radel et al.[23] introduced a downscaled filtration setup for an optical laboratory centrifuge which is based on the setup published by Loginov et al.[24] for investigating filtration properties on a small scale.

To model the settling and filtration process, the flux density function can be used. The flux density function for settling processes was introduced by Kynch[25] and amended by Tiller[26] for compressible sediments. He et al.[27] analyzed and modeled the hindered settling of disk shaped colloids and investigated the influence of particle orientation on settling velocity. Calculating values for the flux density function for solids volume fractions above the gel point from permeability data of filter cakes or sediments was added by Bürger et al.[28] The gel point describes the transition from a suspension to a particulate network. The flux density function is only dependent on the solids volume fraction and describes the settling and permeation properties of a particle system. In numerical simulations of settling or filtration processes, the flux density function combined with the compressible yield stress are useful input parameters to model the whole separation process.

2 | METHODS

2.1 | Particle system

This study considers three different lysozyme crystal systems (isometric, rod-like and needle shaped) and the commercially not available crystal system alcohol dehydrogenase (ADH) from *L. brevis*. Precipitated hen egg-white lysozyme is obtained from Ovobest (Germany), the ADH enzyme is kindly provided by Prof. Weuster-Botz from the institute of biochemical engineering at the Technical University of Munich. Exemplary microscopy images of the crystal systems can be seen in Figure 1.

The crystallized proteins for needle shaped lysozyme, rod-like lysozyme and ADH are kindly provided by Prof. Kind from the institute of thermal process engineering at Karlsruhe Institute of Technology. Those crystals are produced using a low temperature vacuum evaporation process described in detail by Barros Groß and Kind.[29,30] Whereas isometric and ADH crystals grow at 297 K, the rod-like lysozyme crystals are produced at 308 K. Needle shaped lysozyme crystals require additional sodium chloride at a mass fraction of at least 0.03 in the crystallization buffer. Otherwise, the procedure is analogous to the rod-like crystals at a temperature of 297 K.

The production of isometric lysozyme crystals is achieved with displacement crystallization and hence requires two stock solutions. Stock solution A is a 25 mmol acetic acid buffer at pH 4.0. Stock solution B contains 80 g L^{-1} NaCl additionally. 100 g L^{-1} lysozyme are dissolved in 125 mL stock solution A and gently stirred with a blade stirrer at 350 rpm. A membrane pump adds 125 mL stock solution B to the mixture at a rate of 1 mL min^{-1}. The whole crystallization process takes about 16 h to reduce the supersaturation and to reach equilibrium.

Additionally, for the analysis of filtration behavior, the particle and supernatant properties density and viscosity must be known. Those parameters are shown in Table 1. The solid density of crystalline lysozyme is obtained from literature.[31] In house measurements with Mettler Toledo Densito 30PX yield the liquid densities of the continuous, particle free phases using the oscillating tube method according to EN ISO 15212-1.[32] The solid density of ADH crystals is measured with gas pycnometer MP 1305 (Micromeritics GmbH, Germany).[33] Liquid viscosity is obtained with falling sphere viscometry.

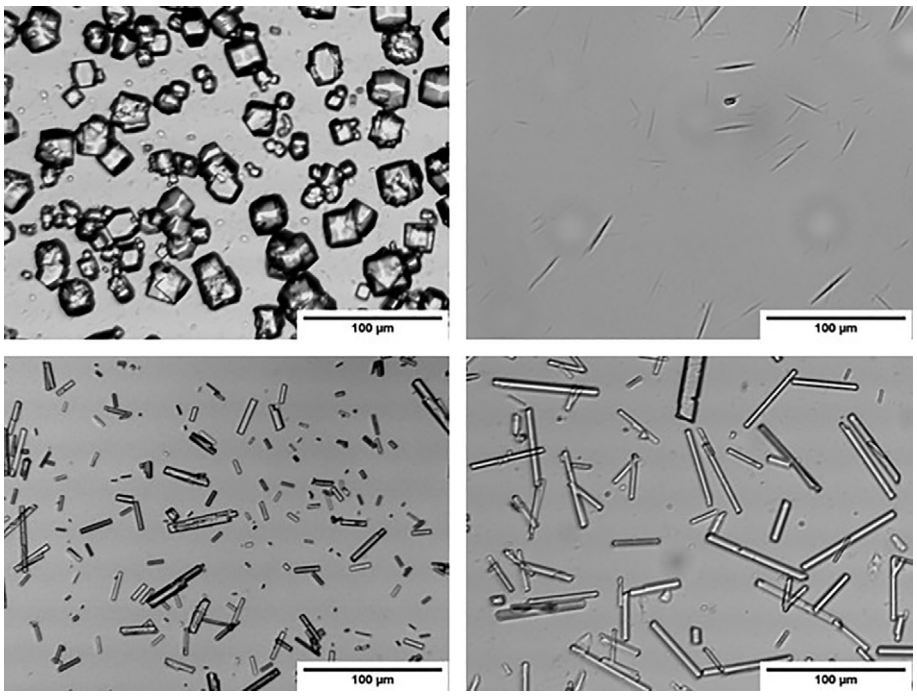

FIGURE 1 Microscopy images of the used protein crystals. Top left: isometric lysozyme, top right: needle shaped lysozyme, bottom left: rod-like lysozyme, bottom right: ADH crystals

TABLE 1 Material properties of the crystalline systems

Particle system	Density solid ρ_s (kg m^{-3})	Density liquid ρ_l (kg m^{-3})	Dyn. Viscosity η (mPa s)
Lysozyme isometric	1236	1023	1.19
Lysozyme rod-like	1236	1023	1.19
Lysozyme needle	1236	1029	1.19
ADH	1250	1026	1.92

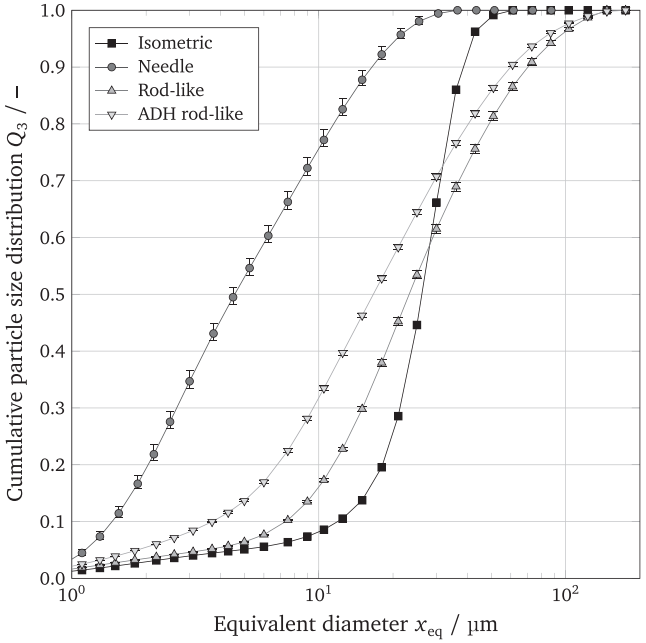

FIGURE 2 Cumulative particle size distributions of the crystalline particles obtained with laser diffraction

Figure 2 shows the cumulative particle size distributions Q_3 of each crystalline system measured in suspension with Sympatec (Germany) Helos laser diffractometer H0309. Due to its measurement principle, laser diffraction gives the equivalent diameter of a sphere, which obviously is only a rough characterization for elongated particles like needles or rods. However, it is still possible to compare the different particle systems relative to each other. Error bars in Figure 2 indicate the minimum and maximum value of three independent repeated measurements.

2.2 | Settling experiments

The settling velocity of particle collectives depends on the solids volume fraction ϕ, which is defined as

$$\phi = \frac{V_s}{V_T} = \frac{V_s}{V_s + V_p} = 1 - \epsilon, \tag{1}$$

with V_s, V_T, V_p as the solids volume, total volume and volume of the void. ϵ is the porosity which is commonly used in the characterization of particulate networks. For low solids volume fractions the particles settle individually depending on density (ρ) and diameter (x). In the case of spherical particles, Reynolds numbers below 0.25 and Newtonian fluids the velocity equals

$$v_s = \frac{(\rho_s - \rho_l) g x^2}{18\eta} \tag{2}$$

which is the Stokes law.[12] With increasing solids volume fraction, the settling regime changes from single particle over swarm to zone settling. In the last regime, most particles have the same settling velocity independent of their diameter. Typically, a sharp transition of clear liquid to suspension, the separation front, develops.[34,12] In broad sized distributions coarse particles might still settle faster than the remaining particles which leads to underestimation of the mean settling velocity. To account for the influence of solids volume fraction on the settling velocity several enhancements to Stokes law in Equation (2) have been introduced in the literature. One common amendment was by Richardson and Zaki[34]

$$v_{rz} = v_s (1 - \phi)^m \tag{3}$$

with the parameter m being a function of the Reynolds number and v_{rz} as the hindered settling velocity. For monodisperse and spherical particles and creeping flow conditions m equals 4.65.

By tracking the separation front over time, settling velocity of the particle system is easily characterized. A typical experiment uses settling columns with different initial solids volume fractions as depicted in Figure 3. The settling velocity is evaluated at the very beginning of the settling process when the solids volume fraction is still homogeneous and equal to the initial solids volume fraction. To measure the settling velocity, the position of the separation front (interface between clear liquid and suspension) is traced over time. To do this, the sample is placed in a small transparent cuvette and the separation front is traced via light transmission. For rapidly settling particle systems, the LUMiReader® instrument (LUM GmbH, Germany) is used, which operates in the earth gravity field. The photocentrifuge LUMiSizer® (LUM GmbH, Germany) uses the centrifugal field (at 500 rpm in this work) to increase the velocity of slowly settling particle systems and allows the characterization of such systems in a reasonable time. For the detailed measurement principle please refer to Lerche and Sobisch.[35]

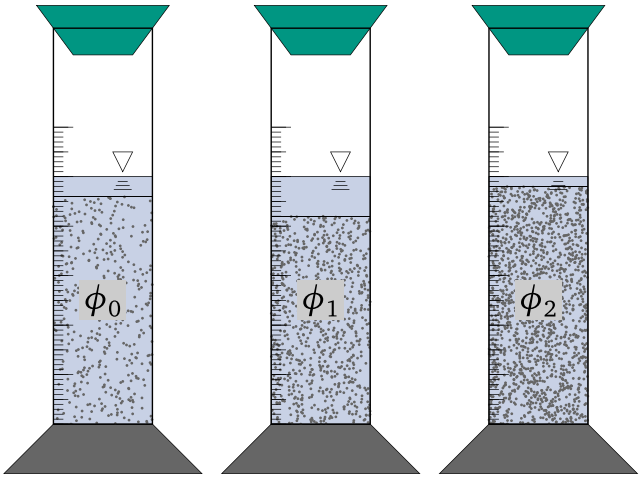

FIGURE 3 Settling columns with different initial solid volume fractions after the same settling time [Color figure can be viewed at wileyonlinelibrary.com]

Because the settling velocity in the centrifugal field is higher than in earth gravity (g), we have to divide the obtained settling velocity from the centrifuge by the relative centrifugal acceleration

$$Z = \frac{r_1 + r_0}{2}\frac{\omega^2}{g}, \tag{4}$$

with r_0 and r_1 as the initial and final distance of the separation front from the centrifuge center and ω as angular velocity.

To create suspensions with different solids volume fractions, addition or removal of supernatant from the initial stock suspension is necessary. Adding supernatant to the crystal stock suspension creates crystal suspensions with lower solids volume fractions. To increase solids volume fraction, a defined volume of supernatant was removed from samples centrifuged at low rotation speeds. Thus, no crystal breakage occurs and redispersing the sediment in remaining supernatant is easy. The optical centrifuge holds up to 12 cuvettes enabling the parallel measurement of the separation front for different solids volume fractions. One important requirement is a clear detectable separation front. Otherwise, it is not possible to determine a single settling velocity. One measurement requires approximately 1.0 mL sample.

2.3 | Filtration experiments

Filtration is a common technique to separate solids from liquids. In dead end cake filtration the particles are held back by a porous filter medium, like a porous membrane or a filter cloth while the filtrate passes through the filter medium. The retained particles on the filter medium first form a thin layer and build particle bridges, then a filter cake. This filter cake may retain particles even smaller than the pores of the filter medium. Often, the chosen pore size of the filter medium is larger than the particles to avoid clogging and to keep the filter medium resistance (R_m) low. The risk of clogged pores is maximal when the particle sizes are in a similar range as the pore sizes because then the particles fit into the pores.[12] In this study, however, the chosen pore size is much smaller than the particles to avoid filtrate pollution and clogging. This allows us to assume that all particles are retained at the cost of a higher filter medium resistance.

Darcy's law connects the pressure drop Δp, filter area (A_m), volume flow rate ($\dot{V}$) and the resistance against permeation (R) with each other. For constant pressure filtration Darcy's law follows

$$\frac{\mathrm{d}V}{\mathrm{d}t} = \frac{\Delta p A_m}{\eta R}. \tag{5}$$

The resistance is typically split into the resistance of the filter medium and resistance of the filter cake (R_c). The resistance of the filter cake changes with its height (h). Thus, for better comparability, the resistance is normalized with either its height or its mass

$$\alpha_h = \frac{R_c}{h_c} = K^{-1}, \tag{6}$$

$$\alpha_m = \frac{\alpha_h}{\phi_c \rho_s}. \tag{7}$$

The reciprocal value of the height specific resistance is the height specific permeability (K).

If the material is incompressible, resistance and solids volume fraction are constant. In the case of compressible material behavior those parameters increase with higher pressure. Compressible material behavior can occur due to particle rearrangement, destruction of card house structures in the case of elongated particles, elastic and plastic deformation or breakage.[13]

To model resistance and solids volume fraction for compressible filter cakes Tiller and Kwon[15] proposed the equations

$$\alpha = \alpha_0 \left(1 + \frac{p}{p_0}\right)^N, \tag{8}$$

$$p = p_0 \left(\left(\frac{\phi}{\phi_0}\right)^\gamma - 1\right), \tag{9}$$

$$\phi = \phi_0 \left(1 + \frac{p}{p_0}\right)^\beta. \tag{10}$$

Equations (9) and (10) can be transformed into each other. The exponent parameters N, γ, and β are fitted to experimental data. Parameters p_0, α_0, and ϕ_0 are usually set to the first available measurement point. With the sum of exponents N and β the compressibility of the particle network is characterized.[13] For N, fitting to mass specific or height specific resistance results in different values. To use Alles and Anlauf's classification scheme, we sum N and β with the values from the height specific resistance. Below one the system is identified as

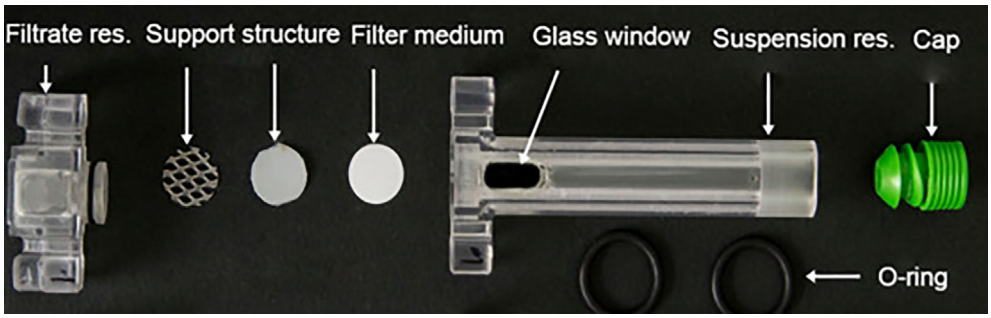

FIGURE 4 3D printed filtration cell [Color figure can be viewed at wileyonlinelibrary.com]

compressible, between one and two as highly compressible and above two as super compressible.[13]

Since new engineered protein crystal suspensions are only available at low volumes (about 1 mL), standard filtration experiments using a pressure nutsche filter are not possible. Although hen egg lysozyme is easily available, ADH from *L. brevis* is not. Therefore, experiments are carried out using an in house 3D printed filtration cell which is depicted in Figure 4. The cuvette consists of two parts. The bottom part catches the filtrate (Figure 4, left), the upper part holds the suspension and the filter cake (Figure 4 right). Between those two parts sits the support structure and the filter medium. The filter area is $A_m = 51.65\,\mathrm{mm}^2$. The assembled cuvette is placed in the LUMiSizer® centrifuge and filtration is traced in situ by light transmission on the cake side. For easier and quicker analysis, the permeation of filter cakes was measured instead of the whole filtration process. The derived equation by Loginov et al.[36]

$$\ln\left(\frac{r_c + r_m - h_l}{r_m - r_c + h_l}\frac{r_m - r_c + h_{l,0}}{r_m + r_c - h_{l,0}}\right) = \frac{\rho_l \omega^2 r_m}{\eta(R_m + (r_m - r_c)\alpha_h)} t, \tag{11}$$

connects the distance from the centrifuge center of the membrane r_m, the filter cake top r_c and the liquid height above the filter cake h_l with material and process properties. From this equation the integral height specific resistance of the filter cake is obtained. For the detailed working principle of the cuvette and data analysis please refer to Radel et al.[23] and Loginov et al.[36] In centrifugal filtration the pressure on the filter medium does not remain constant, but decreases with descending fluid height. Hence, all filtration related pressures mentioned are mean pressures during the filtration process.

For permeation experiments in this study, Pall (Germany) Supor® membranes with a nominal pore size of 0.2 μm and a resistance of 2.1×10^{10} – 3.6×10^{10} m^{-1} are used.[23]

To build the filter cake approximately 500 μL of crystal suspension are filled into the cuvette and centrifuged. For the permeation experiments 300– 400 μL of supernatant are gently added on the top of the prebuilt filter cake with an Eppendorf (Germany) pipette. The liquid is permeated through the filter cake at a defined rotation speed and the progress is tracked. This is repeated for different rotation speeds up to 4000 rpm which is the maximum possible speed.

2.4 | Flux density function

For obtaining the flux density function (f_{bk}) of protein crystals, centrifugal settling and filtration as described in the previous section is used.

In the case of solids volume fractions below the gel point ($\phi_0 < \phi_g$), a common method to measure the flux density function is to observe the settling velocity v_s at the very beginning of the settling process when the solids volume fraction is almost equal to the initial solids volume fraction ϕ_0. The gel point marks the transition from a suspension to a particulate network.

Using Kynch's[25] relation of the flux density function for a closed system

$$f_{bk} = -\phi_0 v_s \text{ for } \phi_0 < \phi_g \text{ and } t \to 0, \tag{12}$$

allows calculating f_{bk} directly from the settling velocity v_s and the known initial solids volume fraction ϕ_0. The standard experimental setup to obtain the settling velocity is explained in Section 2.2 and can be seen in Figure 3, which also qualitatively shows the effect of the solids volume fraction on the settling velocity.

Measuring and tracing the separation front with an optical centrifuge allows to speed the measurement up and to substantially reduce the amount of required sample volume compared to using settling columns. This however means we have to alter Equation (12) to

$$f_{bk} = -\phi_0 \frac{v_s}{Z} \text{ for } \phi_0 < \phi_g \text{ and } t \to 0. \tag{13}$$

Using the resistance of a sediment or filter cake, values for flux density function above the gel point are calculated with

$$f_{bk} = -\frac{\Delta\rho g \phi^2}{\alpha_h \eta} \tag{14}$$

where α_h is a function of ϕ. Determining the mean solids volume fraction and mean height specific filtration resistance with the filtration cell described in Radel et al.[23] is directly possible from the same measurement.

Ideally, joined flux density data obtained from settling and permeation experiments have only a small gap at the gel point. Obviously, the flux density function is significantly higher when considering permeation than during settling.

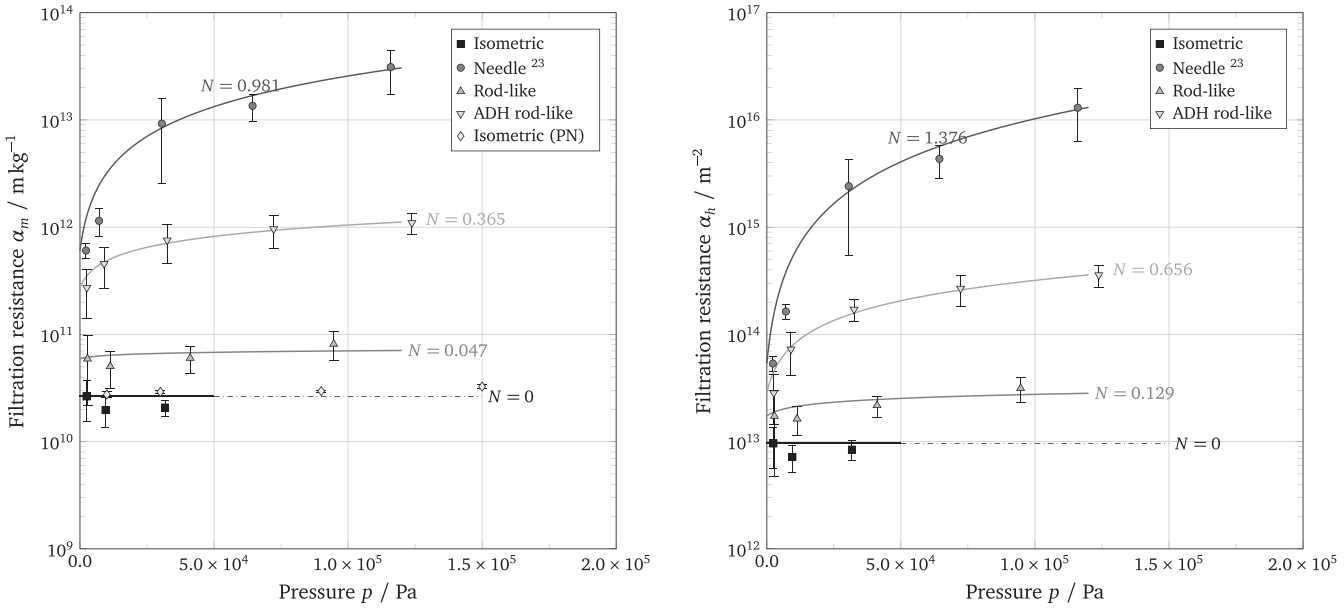

FIGURE 5 Left: mass specific filtration resistance for three lysozyme crystal shapes and rod-like alcohol dehydrogenase crystals; right: height specific filtration resistances for three lysozyme crystal shapes and rod-like alcohol dehydrogenase crystals; The data for needle shaped crystals was published in Radel et al.[23]; solid lines are model calculations according to Tiller and Kwon[15]

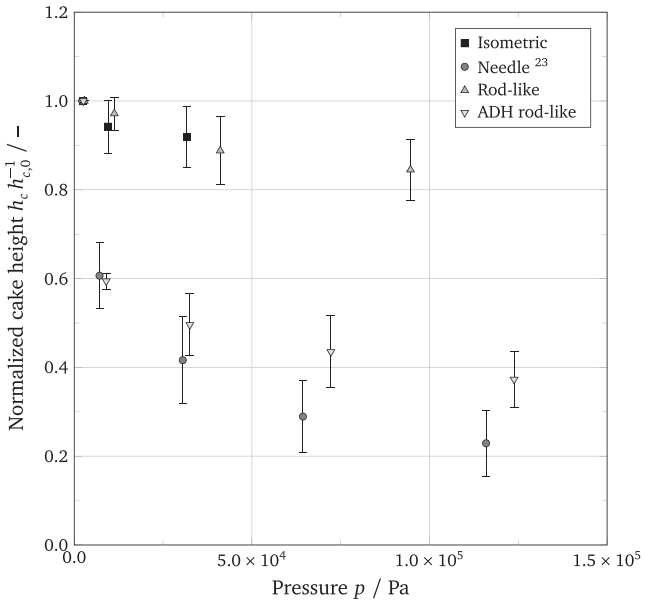

FIGURE 6 Filter cake height of the three lysozyme crystal shapes and rod-like ADH crystals

3 | RESULTS AND DISCUSSION

3.1 | Permeation of filter cakes

3.1.1 | Filter cake resistance

The mass specific filtration resistance obtained from permeation experiments in the centrifuge are shown in Figure 5 left and corresponding height specific resistances are shown on the right-hand side of Figure 5. To compare the different protein crystals with each other, the mass specific resistance is more suitable than the height specific resistance because the resistance is normalized with the particle mass. As can be seen from Figure 5 left, the resistances of isometric and rod-like lysozyme crystals are the lowest with about 2.5×10^{10} and 5×10^{10} m kg^{-1}. Those two systems also show a low dependency of the resistance on pressure which indicates low compressibility. The highest possible pressure for the isometric crystals is below 0.5×10^5 Pa resulting in only three data points. At higher revolutions the start-up of the centrifuge takes too long so that all the liquid is already permeated before the desired revolutions per minute have been reached. Therefore, results obtained with a VDI 2762[22] nutsche filter (diamonds, Isometric PN) are shown for comparison. As can be seen, the results from the pressure nutsche are in very good agreement with the three data points from centrifugal filtration. Although the resistance of rod-like lysozyme crystals is slightly larger than the resistance of isometric crystals, overall both systems offer low resistance and are hence easy to filter. For rod-like ADH crystals on the other hand the resistance is about one order of magnitude larger ranging from 2.7×10^{10} – 1.1×10^{11} m kg^{-1} and shows a slight dependency on the pressure. This indicates compressible material behavior and less efficient filtration.

Needle shaped lysozyme crystals show the highest resistances in the range of 6.1×10^{11} – 3.1×10^{13} m kg^{-1} spreading over two magnitudes. Obviously, this means the filtration process is quite slow compared to the other crystalline systems. Since the resistance increases strongly at higher pressures, the process does not become much faster or efficient when using higher filtration pressures. An increase in resistance this large may be explained by destruction of card house structures in the filter cake and is also a strong indicator for particle breakage.[12]

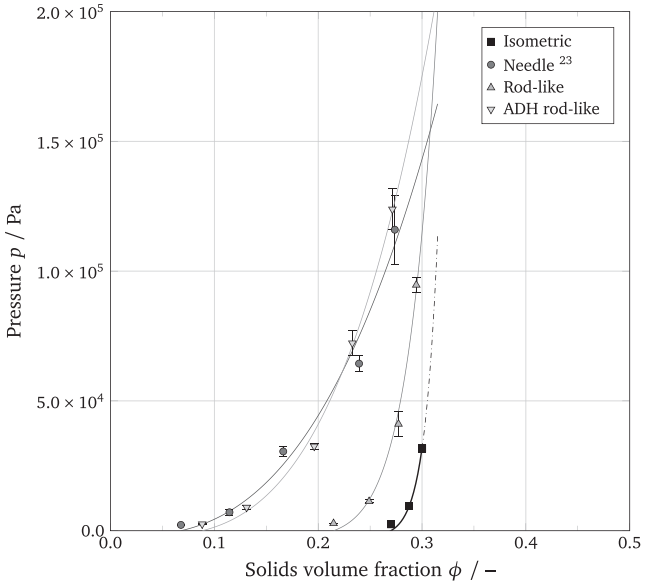

FIGURE 7 Filtration pressure of the crystalline systems dependent on the solids volume fraction

The solid lines show the calculated curves according to Tiller and Kwon[15] from Equation (8). For the isometric lysozyme crystals the extrapolated values are shown in the dash dotted curve. As can be seen, the curves give a good representation of the measurement data. The corresponding values for the exponent N ranges from 0 for the isometric crystals to 0.981 for the lysozyme needles. This also shows the large differences in filter cake compressibility for the different particle systems.

However, to characterize compressibility and to calculate the flux density function, the height specific resistance on the right-hand side of Figure 5 is more suitable because it can be directly inserted into Equation (14). As can be seen, the gap between ADH and the lysozyme crystals is much smaller at low pressures but the tendency is the same. The model fits are calculated analogous to the left-hand side of the Figure with values of N ranging from 0 for the isometric crystals over 0.129 for rod-like to 0.656 for ADH to over 1.376 for needle shaped crystals. Those fits also provide a good representation of the measured data points.

3.1.2 | Filter cake height

The filter cake height of the crystalline systems is directly available from the measurements with the filtration cell because the cake position is always visible and provides a characteristic drop from high to almost zero transmission in the transmission profiles. In Figure 6 the normalized filter cake heights over filtration pressure for the investigated crystal systems are shown. As can be seen from Figure 6, the tendency towards slightly smaller cake heights with increasing pressure is observed for rod-like lysozyme crystals. The same is true for rod-like ADH crystals but the tendency is much more distinct. The most significant decrease in filter cake height is again observed for the needle shaped lysozyme crystals. For those crystals the height decreases from 1.8 mm at 0.22×10^5 Pa to 0.39 mm at 1.16×10^5 Pa which is 21 % of the initial cake height.

In the case of ADH crystals, the small amount of sample available and the low initial solids volume fraction of the sample are the reasons why small portions of the initial ADH suspension were centrifuged at low centrifugal forces to concentrate the particles without causing breakage or crystal aggregation. After careful removal of the supernatant from the centrifuged sample, the solids volume fraction of the now concentrated suspensions scatters. Therefore, the initial cake heights and initial solids volume fractions for ADH are scattered over a wider range than the lysozyme crystals.

The data points also scatter more at lower pressures because the particles tend to partially smear the glass window of the filtration cell, resulting in a more skewed drop in transmittance and thus increasing the uncertainty of the filter cake position.

TABLE 2 Exponents of the fits according to Tiller and Kwon[15] from Equations (8)–(10)

Crystal system	$N(\alpha_h)$	β	γ	$N+\beta$
Isometric	0	0.038	25.003	0.04
Needle	1.376	0.356	2.806	1.73
Rod-like	0.129	0.089	11.173	0.22
ADH	0.656	0.288	3.469	0.94

3.1.3 | Filtration pressure

The knowledge of cake height allows to calculate the corresponding integral solids volume fraction in the filter cake. The filtration pressure vs. solids volume fraction is depicted in Figure 7. For the more compressible systems (needle lysozyme and ADH) the curves show a slow increase of pressure with higher solids volume fractions. In the case of the more incompressible particle systems (isometric and rod-like lysozyme) the increase in pressure is much steeper. For an ideal incompressible particle system the pressure would jump from zero to infinity at the gel point.

The calculated fits according to Equation (9) show good agreement with measurement results. For the isometric crystals the extrapolated values of the dash dotted curve might not be completely accurate. In general, extrapolating is critical due to the exponential nature of the pressure on solids volume fraction dependency. Also, particle systems typically have a maximum solids volume fraction $\phi_{\max}$ at which further compression is impossible. This is currently not reflected in the applied model.

Table 2 shows the calculated parameters for the fit exponents and the sum of $N(\alpha_h)+\beta$. This sum is useful to classify the compressibility of the four particle systems according to Alles and Anlauf.[13] The isometric crystals are considered incompressible with an exponent

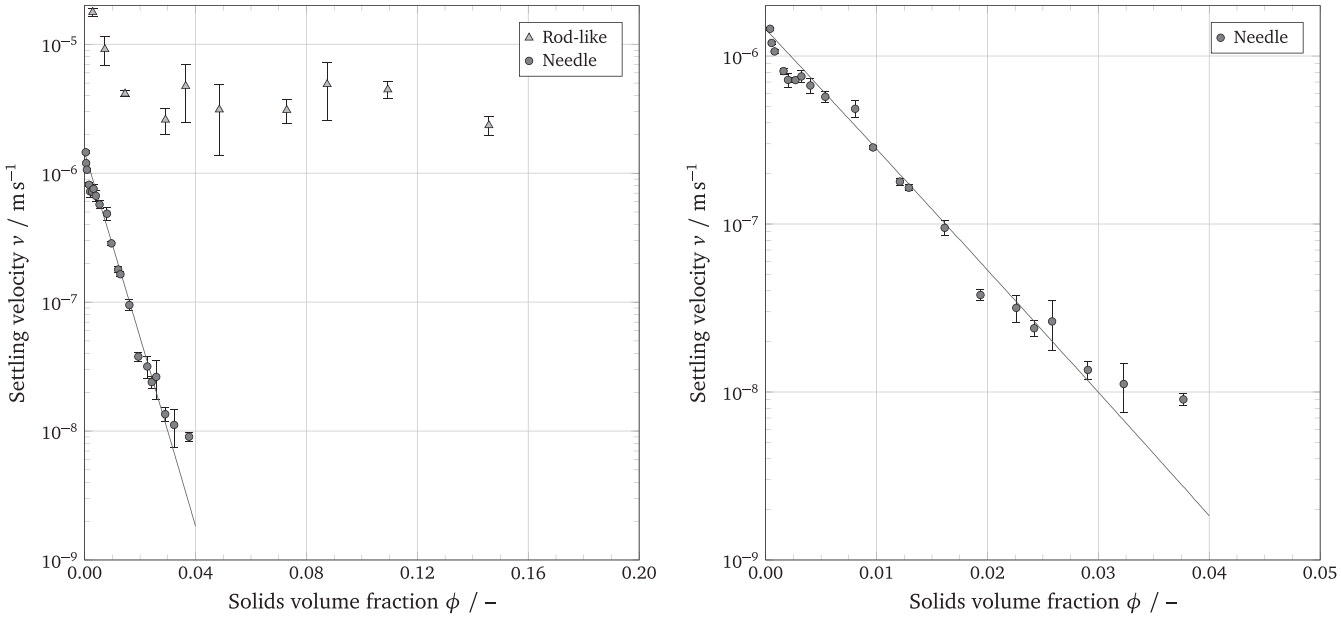

FIGURE 8 Settling velocities for rod-like lysozyme crystals (left, triangles) and needle shaped lysozyme crystals (circles); Velocities for needle shaped lysozyme are converted to earth gravitation. On the right-hand side the settling velocities for the needle shaped crystals at smaller solids volume fractions are shown

sum of 0.04. Rod-like lysozyme and ADH crystals are compressible particle systems, with ADH being significantly more compressible than rod-like lysozyme. Needle shaped lysozyme with a sum of 1.73 is highly compressible and close to super compressibility.[23]

From those results it becomes evident that the particle shape of the four crystal systems has a high influence on filterability. The best filtration properties exhibit isometric and rod-like lysozyme crystals because they have low filtration resistance and thus enable fast filtration. Also, those particle systems have high solids volume fractions which means less residual moisture in the filter cake and hence better dewatering properties. ADH and needle shaped lysozyme crystals on the other hand show compressible material behavior and have high resistances compared to the other two particle systems. The solids volume fraction at lower pressures is much smaller for those particle systems which means that more fluid remains in the pores of the filter cake. Thermal drying of filter cakes with crystalline systems is difficult because the dissolved protein in the pore fluid crystallizes when the fluid evaporates and thus blocks the pores needed to transport the evaporated gas.

The comparison of Figures 2 and 5 shows a big influence of particle shape, size and distribution on filter cake resistance and compressibility. The high compressibility of needle shaped lysozyme and rod-like ADH possibly follows from the formation of card house structures that recompress and compact at higher pressure. This leads to the sharp increase in cake resistance. For the needle shaped lysozyme, moreover, particle breakage is suspected at higher pressures, which can also occur with ADH. In the case of isometric and rod-like lysozyme, there is no or very little compressibility. The differences between rod-like lysozyme and ADH in compressibility behavior are due to two reasons. First, the particle size distribution of ADH is broader and somewhat shifted to smaller crystals, which favors compression. Second, for technical reasons, the initial solids volume fraction for lysozyme is much higher than for ADH, which may lead to a different cake structure.

3.2 | Settling

For two of the discussed crystal systems settling velocities in earth gravity (rod-like lysozyme) and in the centrifugal field (needle shaped lysozyme) have been determined. The isometric crystal suspension did not show a clear separation front so that the results are inconclusive. The available sample volume for ADH did not allow a thorough analysis of settling behavior.

Figure 8 shows on the left-hand side the settling velocities for different solids volume fractions of needle shaped and rod-like lysozyme crystals. On the right-hand side the settling velocities for the needle shaped lysozyme crystals are shown enlarged to better visualize the settling at low solids volume fractions.

To make the results from centrifugal settling experiments comparable with the other particle system, the velocities have been recalculated according to

$$v_g = \frac{v_C}{Z}. \tag{15}$$

with v_C being the settling velocity in the centrifugal field and v_g being the settling velocity in earth gravity. The definition of Z is given in Equation (4).

For both particle systems the settling velocity decreases with increasing solids volume fraction. In the case of rod-like crystals the

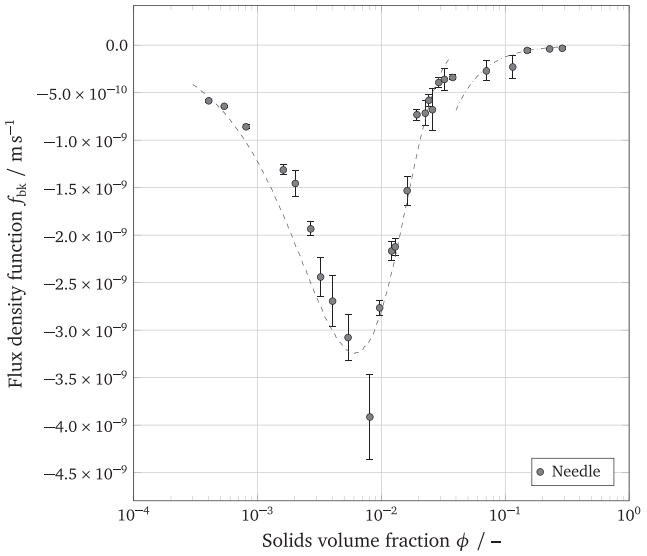

FIGURE 9 Flux density function for needle shaped lysozyme particles

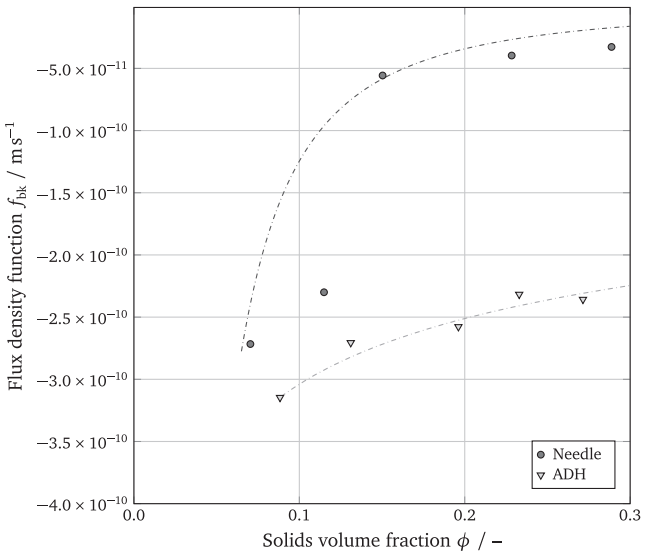

FIGURE 10 Flux density function for needle shaped lysozyme and ADH at solids volume fractions above the gel point

maximum settling velocity is 17.7×10^{-6} m s $^{-1}$ at the lowest solids volume fraction of 0.003. The velocity then quickly drops to around 4.0×10^{-6} ms^{-1} at solids volume fractions above 0.014 and then fluctuates around this value for solids volume fractions up to 0.146.

In the case of the lysozyme needles, the reduction in settling velocity is much bigger. The initial settling velocity is about 1.45×10^{-6} m s $^{-1}$ at a solids volume fraction of 0.0004. Settling velocity then slowly decreases to a final value of about 0.003×10^{-6} m s $^{-1}$ at $\phi = 0.019$ and remains almost constant till the maximum solids volume fraction of 0.038. At the lowest solids volume fraction for the rod-like crystals ($\phi = 0.003$) the corresponding settling velocity for the needles amounts to 0.74×10^{-6} m s $^{-1}$ which is only 4.1 % of the rod-like crystals settling velocity at the same solids volume fraction.

The decrease of settling velocities in both particle systems is due to hindered settling in a particle collective. At low solids volume fractions single particle settling as described by Stokes is thus much faster than hindered settling at higher solids volume fractions.

The maximum solids volume fraction, which could be achieved with concentration of the particle systems, is for the rod-like crystals with 0.146 almost four times bigger than for the needle shaped crystals with 0.038. This also reflects in the big gap of solids volume fraction for those both crystal shapes in Figure 7. The gel point for lysozyme needles must hence be much lower than for rod-like lysozyme crystals.

Also, the total drop in settling velocity is for needle shaped lysozyme crystals with a factor of 161 much larger than for the rod-like crystals where the settling velocity drops at a factor of about 7.5. The influence of solids volume fraction on settling velocity is thus for the lysozyme needles much more dominant than for the rod-like crystals. It is also interesting to see that with settling experiments the solids volume fraction of lysozyme needles reaches 0.038 but in filtration this particle system is compressed to a solids volume fraction of 0.274 (see Figure 7). This corresponds to a 7.2-fold increase in solids volume fraction. This can be explained by the destruction of card house structures in the filter cake to a more compact cake and also by crystal breakage. Cornehl et al.[11] have analyzed lysozyme crystal breakage. They found that even at low pressures in typical filtration processes, crystal breakage occurs which worsens filtration and dewatering properties.

The solid line in Figure 8 right shows a modified fit based on Richardson and Zaki[34] (see Equation (3)). Since the model of Richardson and Zaki assumes spherical particles, adjustments for needle shaped particles are necessary. Instead of using the default exponent 4.65, the exponent m is calculated with respect to measured experimental data and gives 163.4. Such a curve cannot be calculated for the rod-like particles because of the fluctuating settling velocities in the range of solids volume fractions from 0.04 to 0.147. A possible explanation is the transition from unstructured, randomly orientated rods at low solid volume concentrations towards an orientated particle collective due to steric hindering at higher solids volume fractions. He et al.[27] found and modeled a similar effect of particle orientation on settling velocity for colloidal disk-shaped particles.

3.2.1 | Flux density function

With the results from the previous sections, especially with the calculated fit models from Richardson and Zaki[34] and Tiller and Kwon,[15] the flux density function can be calculated as follows.

$$f_{bk} = \begin{cases} -\phi v_s (1-\phi)^m & \text{for } \phi < \phi_g \\ -\dfrac{\Delta\rho g \phi^2}{\alpha_{h0}\left(\left(\frac{\phi}{\phi_0}\right)^{\gamma}\right)^N \eta} & \text{for } \phi_g \le \phi \end{cases}. \tag{16}$$

Figure 9 shows the complete flux density function for the needle shaped particle system. The gel point is not exactly known but

expected to lie somewhere between 0.03 and 0.06. The dashed line in Figure 9 is the calculated flux density function according to the modified Richardson and Zaki model (first segment of Equation (16)). The dash dotted line is calculated based on permeation data with the models of Tiller. The last five data points in Figure 9 are obtained with permeation experiments, the other data points at lower solids volume fractions are determined with settling experiments.

Figure 10 shows the flux density function for solids volume fractions above the gel point for needle shaped lysozyme and ADH crystals calculated from permeation data. As can be seen the flux density of ADH crystals is much smaller than the flux density of needle shaped lysozyme which is due to the lower filter cake resistance of ADH. The model describes the measured data well except for the second data point of the needle shaped lysozyme.

The flux density function allows to model the settling and permeation behavior of a particle system only in dependency of the solids volume fraction. This is especially useful for processes in which both effects play a significant role. Also in simulation models, for instance in Bürger and Concha,[37] the flux density function is used as an input parameter for the simulation of settling processes.

4 | CONCLUSION

The settling and permeation behavior for different protein crystal systems can be analyzed on a small scale using a 3D printed filtration cell and an analytical optical centrifuge. The crystal shape has a big influence on the filtration and settling properties. Being able to characterize filtration and settling on a small scale allows testing different crystal shapes or crystal modifications early in process development. Using the flux density function, the whole settling and permeation process can be modeled in dependency of the solids volume fraction. For solids volume fractions below the gel point this requires the ability to observe a distinct separation front. This is not possible for all particle systems, but for example in the case of the needle shaped lysozyme crystals. Above the gel point the flux density function can be obtained with permeation experiments on a small scale with only about 300 μL of supernatant per experiment.

As a first step, the flux density function determined on a small scale allows to describe the sedimentation and filtration behavior of different protein crystal systems. The method presented in this article is not limited to proteins but can also be applied to other particle systems that are only available in small quantities during product development. As an outlook, simulations using the flux density function are conceivable, such as filtration in a chamber filter press. The flux density function and the compression resistance serve as input parameters, for example, in adapted models of Bürger et al.[38] and Garrido et al.[39] In material systems where particle breakage occurs in the filter cake, the change in flow resistance is also represented by the flux density function.

ACKNOWLEDGMENTS

The authors thank the German Research Foundation (DFG) for funding the project NI 414/26-1, NI 414/26-2 and the DiSPBiotech Priority Program (SPP 1934). Prof. Kind and Dr.-Ing. Michael Barros-Groß from the institute of thermal process engineering at the KIT are thanked for providing crystalline proteins. Prof. Weuster-Botz and Dr. Phillip Grob of the institute for biochemical engineering at Technical University of Munich are thanked for providing the protein alcohol dehydrogenase from *Lactobacillus brevis*. Open Access funding enabled and organized by Projekt DEAL.

CONFLICT OF INTEREST

The authors declare that there is no conflict of interest to disclose.

AUTHOR CONTRIBUTIONS

Benjamin Radel: Conceptualization; data curation; investigation; methodology; project administration; visualization; writing - original draft; writing-review & editing. **Tu Nguyen:** Conceptualization; data curation; investigation. **Hermann Nirschl:** Conceptualization; funding acquisition; project administration; supervision; writing-review & editing.

NOTATION

LATIN SYMBOLS

A area (mm^2)
f_{bk} flux density function ($m\,s^{-1}$)
g gravity ($m\,s^{-2}$)
h height (mm)
K specific permeability (m^2)
p pressure (Pa)
Q cumulative particle size distribution (−)
R resistance (m^{-1})
r distance from centrifuge center (mm)
t time (s)
V volume (m^3)
v velocity ($m\,s^{-1}$)
x particle diameter (μm)
Z relative centrifugal acceleration (−)

GREEK SYMBOLS

α_h height specific resistance (m^{-2})
α_m mass specific resistance ($m\,kg^{-1}$)
ε porosity (−)
η dynamic viscosity (Pa s)
ω angular velocity (s^{-1})
ϕ solids volume fraction (−)
ϕ_0 solids volume fraction at $p = p_0$ (−)
ρ density ($kg\,m^{-3}$)

SUBSCRIPTS

0 initial value
c filter cake related
g gel point related
l liquid related
m filter medium related
s suspension/solids related

DATA AVAILABILITY STATEMENT

The data that support the findings of this study are available from the corresponding author upon reasonable request.

ORCID

Benjamin Radel https://orcid.org/0000-0001-8479-7288

REFERENCES

1. Jen A, Merkle HP. Diamonds in the rough: protein crystals from a formulation perspective. *Pharm Res*. 2001;18(11):1483-1488.
2. Basu SK, Govardhan CP, Jung CW, Margolin AL. Protein crystals for the delivery of biopharmaceuticals. *Expert Opin Biol Ther*. 2004;4(3):301-317.
3. Hubbuch J, Kind M, Nirschl H. Preparative protein crystallization. *Chem Eng Technol*. 2019;42(11):2275-2281.
4. Hekmat D. Large-scale crystallization of proteins for purification and formulation. *Bioprocess Biosyst Eng*. 2015;38(7):1209-1231.
5. Nowotny P, Hermann J, Li J, et al. Rational crystal contact engineering of lactobacillus brevis alcohol dehydrogenase to promote technical protein crystallization. *Cryst Growth Des*. 2019;19(4):2380-2387.
6. Hermann J, Nowotny P, Schrader TE, Biggel P, Hekmat D, Weuster-Botz D. Neutron and X-ray crystal structures of lactobacillus brevis alcohol dehydrogenase reveal new insights into hydrogenbonding pathways. *Acta Crystallogr F*. 2018;74(12):754-764.
7. Kubiak M, Solarczek J, Kampen I, Schallmey A, Kwade A, Schilde C. Micromechanics of anisotropic cross-linked enzyme crystals. *Cryst Growth Des*. 2018;18(10):5885-5895.
8. Grob P, Huber M, Walla B, et al. Crystal contact engineering enables efficient capture and purification of an oxidoreductase by technical crystallization. *Biotechnol J*. 2020;15(11):2000010.
9. Kubiak M, Storm KF, Kampen I, Schilde C. Relationship between cross-linking reaction time and anisotropic mechanical behavior of enzyme crystals. *Cryst Growth des*. 2019;19(8):4453-4464.
10. Cornehl B, Grünke T, Nirschl H. Mechanical stress on lysozyme crystals during dynamic cross-flow filtration. *Chem Eng Technol*. 2013;36(10):1665-1674.
11. Cornehl B, Overbeck A, Schwab A, Büser JP, Kwade A, Nirschl H. Breakage of lysozyme crystals due to compressive stresses during cake filtration. *Chem Eng Sci*. 2014;111:324-334.
12. Anlauf H. *Wet Cake Filtration: Fundamentals, Equipment, Strategies*. Wiley-VCH: Weinheim; 2020.
13. Alles CM, Anlauf H. Filtration mit kompressiblen Kuchen: Effiziente Konzepte für eine anspruchsvolle Trennaufgabe. *Chem Ing Tech*. 2003;75(9):1221-1230.
14. Tiller FM, Hsyung NB. Unifying the theory of thickening, filtration, and centrifugation. *Water Sci Technol*. 1993;28(1):1-9.
15. Tiller FM, Kwon JH. Role of porosity in filtration: XIII. Behavior of highly compactible cakes. *AIChE J*. 1998;44(10):2159-2167.
16. Tarleton ES. Predicting the performance of pressure filters. *Filtr Sep*. 1998;35(3):293-286.
17. Stickland AD. A compressional rheology model of fluctuating feed concentration during filtration of compressible suspensions. *Chem Eng Sci*. 2012;75:209-219.
18. Stickland AD, Skinner SJ, Cavalida RG, Scales PJ. Optimization of filter design and operation for wastewater treatment sludge. *Sep Purif Technol*. 2018;198:31-37.
19. Wetterling J, Mattsson T, Theliander H. Modelling filtration processes from local filtration properties: the effect of surface properties on microcrystalline cellulose. *Chem Eng Sci*. 2017;165:14-24.
20. Capellades G, Neurohr C, Azad M, et al. A compact device for the integrated filtration, drying, and mechanical processing of active pharmaceutical ingredients. *J Pharm Sci*. 2020;109(3):1365-1372.
21. Dobler T, Buchheiser S, Gleiß M, Nirschl H. Development and commissioning of a small-scale, modular and integrated plant for the quasi-continuous production of crystalline particles. *Processes*. 2021;9(4):663.
22. VDI 2762. *Mechanical Solid–Liquid Separation by Cake Filtration. Standard VDI 2762*. Düsseldorf: Verein Deutscher Ingenieure; 2010.
23. Radel B, Funck M, Nguyen TH, Nirschl H. Determination of filtration and consolidation properties of protein crystal suspensions using analytical photocentrifuges with low volume samples. *Chem Eng Sci*. 2019;196:72-81.
24. Loginov M, Samper F, Gésan-Guiziou G, Sobisch T, Lerche D, Vorobiev E. Centrifugal ultrafiltration for determination of filter cake properties of colloids. *J Membr Sci*. 2017;536:59-75.
25. Kynch GJ. A theory of sedimentation. *Trans Faraday Soc*. 1952;48:166.
26. Tiller FM. Revision of kynch sedimentation theory. *AIChE J*. 1981;27(5):823-829.
27. He P, Mejia AF, Cheng Z, et al. Hindrance function for sedimentation and creaming of colloidal disks. *Phys Rev E*. 2010;81(2):026310.
28. Bürger R, Concha F, Tiller FM. Applications of the phenomenological theory to several published experimental cases of sedimentation processes. *Chem Eng J*. 2000;80(1–3):105-117.
29. Barros Groß M, Kind M. Comparative study on seeded and unseeded bulk evaporative batch crystallization of tetragonal lysozyme. *Cryst Growth des*. 2017;17(6):3491-3501.
30. Barros Groß M, Kind M. From microscale phase screening to bulk evaporative crystallization of proteins. *J Cryst Growth*. 2018;498:160-169.
31. Kundrot CE, Richards FM. Effect of hydrostatic pressure on the solvent in crystals of hen egg-white lysozyme. *J Mol Biol*. 1988;200(2):401-410.
32. EN ISO 15212-1. *Oscillation-type Density Meters—Part 1: Laboratory Instruments. Standard EN ISO 15212-1*. Brussels: European Committee for Standardization; 1999.
33. ISO 12154. *Determination of Density by Volumetric Displacement—Skeleton Density by Gas Pycnometry. Standard ISO 12154*. Geneva: International Organization for Standardization; 2014.
34. Richardson JF, Zaki WN. Sedimentation and fluidisation: Part I. *Chem Eng Res Des*. 1997;75:S82-S100.
35. Lerche D, Sobisch T. Consolidation of concentrated dispersions of nano- and microparticles determined by analytical centrifugation. *Powder Technol*. 2007;174(1–2):46-49.
36. Loginov M, Lebovka N, Vorobiev E. Multistage centrifugation method for determination of filtration and consolidation properties of mineral and biological suspensions using the analytical photocentrifuge. *Chem Eng Sci*. 2014;107:277-289.
37. Bürger R, Concha F. Mathematical model and numerical simulation of the settling of flocculated suspensions. *Int J Multiphase Flow*. 1998;24(6):1005-1023.
38. Bürger R, Bustos M, Concha F. Settling velocities of particulate systems: 9. Phenomenological theory of sedimentation processes: numerical simulation of the transient behaviour of flocculated suspensions in an ideal batch or continuous thickener. *Int J Miner Process*. 1999;55(4):267-282.
39. Garrido P, Concha F, Bürger R. Settling velocities of particulate systems: 14. Unified model of sedimentation, centrifugation and filtration of flocculated suspensions. *Int J Miner Process*. 2003;72(1–4):57-74.

How to cite this article: Radel B, Nguyen TH, Nirschl H. Calculation of the flux density function for protein crystals from small scale settling and filtration experiments. *AIChE J*. 2021;e17378. https://doi.org/10.1002/aic.17378